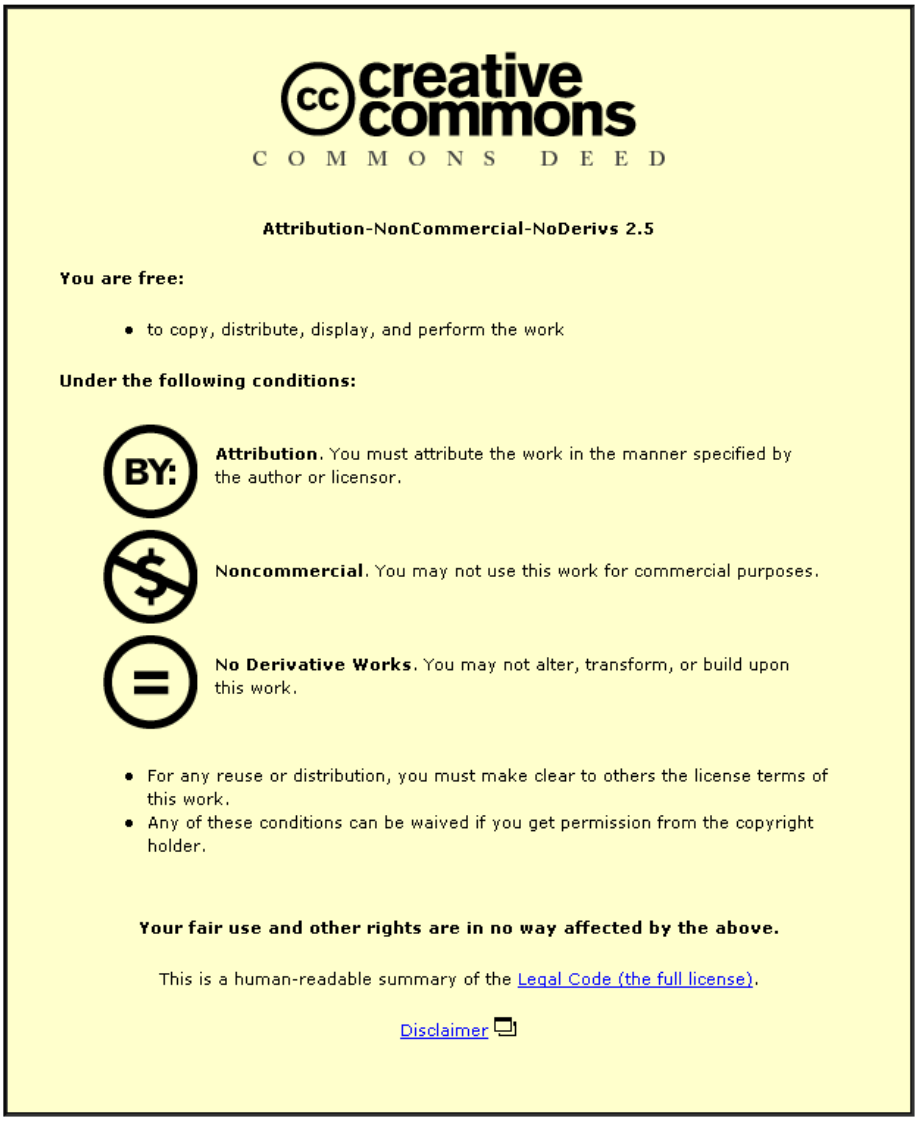

creative commons

COMMONS DEED

Attribution-NonCommercial-NoDerivs 2.5

You are free:

- to copy, distribute, display, and perform the work

Under the following conditions:

Attribution. You must attribute the work in the manner specified by the author or licensor.

Noncommercial. You may not use this work for commercial purposes.

No Derivative Works. You may not alter, transform, or build upon this work.

- For any reuse or distribution, you must make clear to others the license terms of this work.
- Any of these conditions can be waived if you get permission from the copyright holder.

Your fair use and other rights are in no way affected by the above.

This is a human-readable summary of the Legal Code (the full license).

Disclaimer

HARDNESS OF ALUMINA/SILICON CARBIDE NANOCOMPOSITES AT VARIOUS SILICON CARBIDE VOLUME PERCENTAGES

James Wade & Houzheng Wu
Department of Materials, Loughborough University, Leicestershire, LE11 3TU, UK

ABSTRACT

Vickers indentation was employed to measure the microhardness of monolithic alumina and six alumina-based nanocomposites consisting of variable silicon carbide nanoparticle volume percentages of 0.3% to 20%. Indentation tests were performed over a broad range of loads from 0.5N to 40N. The resultant hardness-load curves exhibit cumulative increases in the apparent hardness based on the silicon carbide content and reveal each sample suffers from a prominent indentation size effect (ISE). Herein, we present a comprehensive analysis of this data using Meyer's Law, the proportional specimen resistance model (PSR) and the modified proportional specimen resistance model (MPSR) and employ TEM imagery to detail potential mechanisms by which silicon carbide nano-reinforcements influence the "true hardness" and the ISE.

INTRODUCTION

For nearly a century, microindentation has been a fundamental and widely-accepted method for determining the mechanical property of hardness[1, 2]. In ceramics, irrespective of the indenter characteristics (Vickers, Knoop, Berkovich, Rockwell, Brinell, etc.), the technique is said to provide a quantifiable measurement of resistance to deformation, densification, displacement and fracture[3]. This is achieved by measuring the horizontal and vertical diameters of a diamond-shaped impression generated by a loaded indenter. The hardness (H) is subsequently calculated as a ratio of load to resultant contact area, the equation of which is represented as follows:

$$H = \alpha(P/d^2) \tag{1}$$

where d is an average of the respective diameters of the indent, α is the indenter constant, a number dependant on the geometry of the indenter employed, and P is the load.

Traditionally, during conventional testing both the indenter constant and load would remain as fixed parameters. However, it has been reported in numerous investigations that by increasing the load applied through the indenter a notable decrease in the calculated hardness can be observed[3, 4, 5, 6, 7, 8, 9, 10, 11, 12, 13, 14]. This apparent load-dependency in the eventual hardness values realised through microindentation is referred to as the indentation size effect (ISE) and was initially described through Meyer's Law[15]

$$P = Ad^n \tag{2}$$

where A and n are constants derived via regression analysis of experimental results.

Unfortunately, at present, because of the ISE phenomena, only a superficial hardness value can be obtained from the application of any microindentation technique and whilst Meyer's Law aligns relatively well with the majority of hardness-load curves (H-P), it is still insufficient and unable to address this issue.

Consequently, a range of alternative models have been proposed, including the Hays-Kendall approach[8], the elastic recovery model[9], the proportional specimen resistance model (PSR)[10, 11, 12], the energy-balance approach[3, 11], the modified proportional specimen resistance model (MPSR)[13] and the fractal approach[14].

For brittle ceramic materials, which do not experience the increased complexities of metal-related mechanics such as work hardening and high elastic strain, the PSR (Eq. 3) and MPSR models (Eq.4) have been adopted. These two models, when comparatively assessed against Meyer's Law, exhibit not only an improved curve fitting against the experimental data, but also involve the separation of the load-dependent ISE and the load-independent hardness into two individual terms, a_1 and a_2 respectively. In doing so, what is known as and argued to be the "true hardness"[16] (a_2) can be determined.

$$P = a_1 d + a_2 d^2 \tag{3}$$

$$P = a_0 + a_1 d + a_2 d^2 \tag{4}$$

where a_0 is an additional constant that represents the indenter-induced residual surface stresses.

Whilst a number of comparative studies conducted on several single-crystal and polycrystalline ceramics have remained inconclusive as to the ascendancy of each model[6, 12, 13, 16, 17, 18, 19, 20] speculations concerning the cause of the ISE and the physical meaning associated with the "true hardness" have been widespread.

The a_1 term has been related to various mechanisms, including the energy consumed in the creation of new surfaces[10, 11], the energy required for surface stretching prior to crack initiation[16], interfacial friction resistance[12, 21], bulk elastic recovery[9, 12] and subsurface cracking[22], either inherent or initiated concurrently with the indentation process.

Conversely, the a_2 term has just one interpretation, being ascribed to crack-free plastic deformation. Nevertheless, whilst this has been generally acknowledged, the supporting evidence is sparse. Furthermore, there is a lack of comprehension in regards to the governing factors which control the "true hardness".

In this paper, we report the results of an extensive and meticulous Vickers microindentation study performed on ground and polished monolithic alumina (Al_2O_3) ceramics and alumina/SiC (Al_2O_3/SiC) nanocomposites: the use of which, can be rationalised by considering that one sole variable differentiates each sample, the volume percentage (vol%) of SiC dispersants. Using observational work from earlier studies by one of these authors, we propose that variations in the "true hardness" are dictated by the vol% of SiC and can be attributed to the nano-dispersants capacity to resist the motion of dislocations in the matrix.

EXPERIMENTAL PROCEDURE

In this investigation, a monolithic Al_2O_3 ceramic and six Al_2O_3-based nanocomposites containing 0.3, 1, 3, 5, 10 and 20vol%SiC were prepared via pressureless-sintering and hot-pressing respectively.

An in-depth methodology detailing the manufacture process in full is given in other publications[23]. Briefly though, in order to control the growth of alumina grains and to ensure a mean grain size equivalent to that of the pure Al_2O_3 pressureless-sintered at 1500°C (~3-4μm), all nanocomposites were hot-pressed in a graphite die at between 1550-1720°C for 1hr under a pressure of ~25MPa in flowing argon. In doing so, full densification of all the samples was achieved. The Al_2O_3 powder used was a high purity (99.99% α- Al_2O_3) AKP53 (Sumitomo, Japan) with a sub-micrometre particle size. The SiC nanoparticles were α-SiC powder UF 45 (Lonza, Germany) with an average particles size of ~90nm.

After manufacture, the indentation surfaces of the monolithic Al_2O_3 and Al_2O_3/SiC nanocomposites were machined to produce a smooth surface-finish parallel with the base plane. The samples were positioned onto two flat mild steel blocks (4 samples on each) and held in place by a hard, high strength mounting wax (Testbourne Ltd, Basingstoke, UK). Initial levelling of the surface

was carried out using an Axminster Sieg U2 1000W drill (Axminster Tool Centre, Devon, UK) under the following conditions: Ø60mm diamond (100µm) core drill bit at a rotation speed 450rpm and a feed depth of 10µm per pass. Such coarse grinding was followed by lapping and polishing on a bench mounted KEMET 15 flat-bed diamond lapping machine (Kemet International, Maidstone, UK). Four grades of diamond slurry were applied to 4 separate wheels; 25µm iron wheel, 8µm and 3µm copper wheel, 3µm cloth polishing wheel, and a 1µm cloth polishing wheel. Depending on the wheel, a typical cycle lasted between 30-120 minutes. Once a shiny, polished surface-finish was achieved the samples were cleaned to remove any residual lubricant and/or diamond grit before indentation.

Two Vickers microindenters were employed to generate indents at the various loads. A Mitutoyo HM-124 (Mitutoyo UK Ltd, Andover, UK) was used at loads of 0.05kgf (0.49N), 0.1kgf (0.98N), 0.2kgf (1.96N), 0.3kgf (2.94N), 0.5kgf (4.9N), 1kgf (9.8N), and 2kgf (19.61N). An Innovatest Nexus 4503 (Innovatest Europe, Maastricht, The Netherlands) was then needed for higher loads of 2.5kgf (24.51N), 3.0kgf (29.42N) and 4kgf (39.23N). Both machines boast a load accuracy of <1% at each load. 15 seconds was the elected dwell time. All samples remained on the mild steel blocks during indentation which was performed at room temperature.

The resultant indents were imaged in the SEM. All SEM observations were made using a Carl Zeiss (Leo) 1530 VP; samples were sputter-coated with a thin coating of gold-palladium to prevent charging. Meanwhile, graphic editing software (Adobe Photoshop, USA) was used to determine the horizontal (d_1) and vertical (d_2) diameters in mm. The hardness was calculated using Eq. 1, where α, the indenter specific constant = 1.8544 for a Vickers indenter and the load, P, was in Newtons (N).

All cross-sectioned TEM samples were prepared by ion-milling[23] and TEM analysis was carried out on JEOL200CX and JEOL4000 microscopes.

The load dependent nature of the measured hardness results for both monolithic Al_2O_3 and each of the Al_2O_3/SiC nanocomposites was subsequently analysed against three models: Meyer's Law, the PSR model and the MSPR model.

EXPERIMENTAL RESULTS AND DISCUSSION

The *H-P* curves for the monolithic Al_2O_3 and the Al_2O_3/SiC nanocomposites are displayed in Fig. 1(a). For the purposes of clarity and conciseness, all error bars of plus and minus one standard deviation have been displayed in the adjoining bar chart in Fig. 1(b). As expected, maximum scattering, typically 7–8% of the hardness value, occurred in the fracture-prone unreinforced Al_2O3 and is particularly prevalent at the lower load ranges. As recommended[3, 20], in order to alleviate variance, each of the plotted data points is an average of at least 5 measurements. The typical conditions of the indents measured are presented in the SEM images in Fig. 2.

From Fig. 1(a), it is evident that both the monolithic Al_2O_3 and the Al_2O_3/SiC nanocomposites experience an ISE of varying degrees. Additionally, each sample appears to encounter an abrupt, but continuous plateau in the apparent hardness values collected after ~20N. This is consistent with the hardness transition point hypothesised by Quinn & Quinn[3].

Using the data in Table 1, confirmation that a levelling of the hardness has occurred is achieved by comparatively examining the mean hardness ($H_{plateau}$) across the four loads of the plateau (20N, 25N, 30N and 40N) against the minimum recorded hardness (H_{min}) for each sample. In all cases, these numbers are similar in value, despite the H_{min} being taken from various load points (P_{min}). Whilst not entirely conclusive, it is possible to deduce from this that across the loads of the $H_{plateau}$ the measured hardness has begun to equalise. Meyer's Law may also be employed to confirm this.

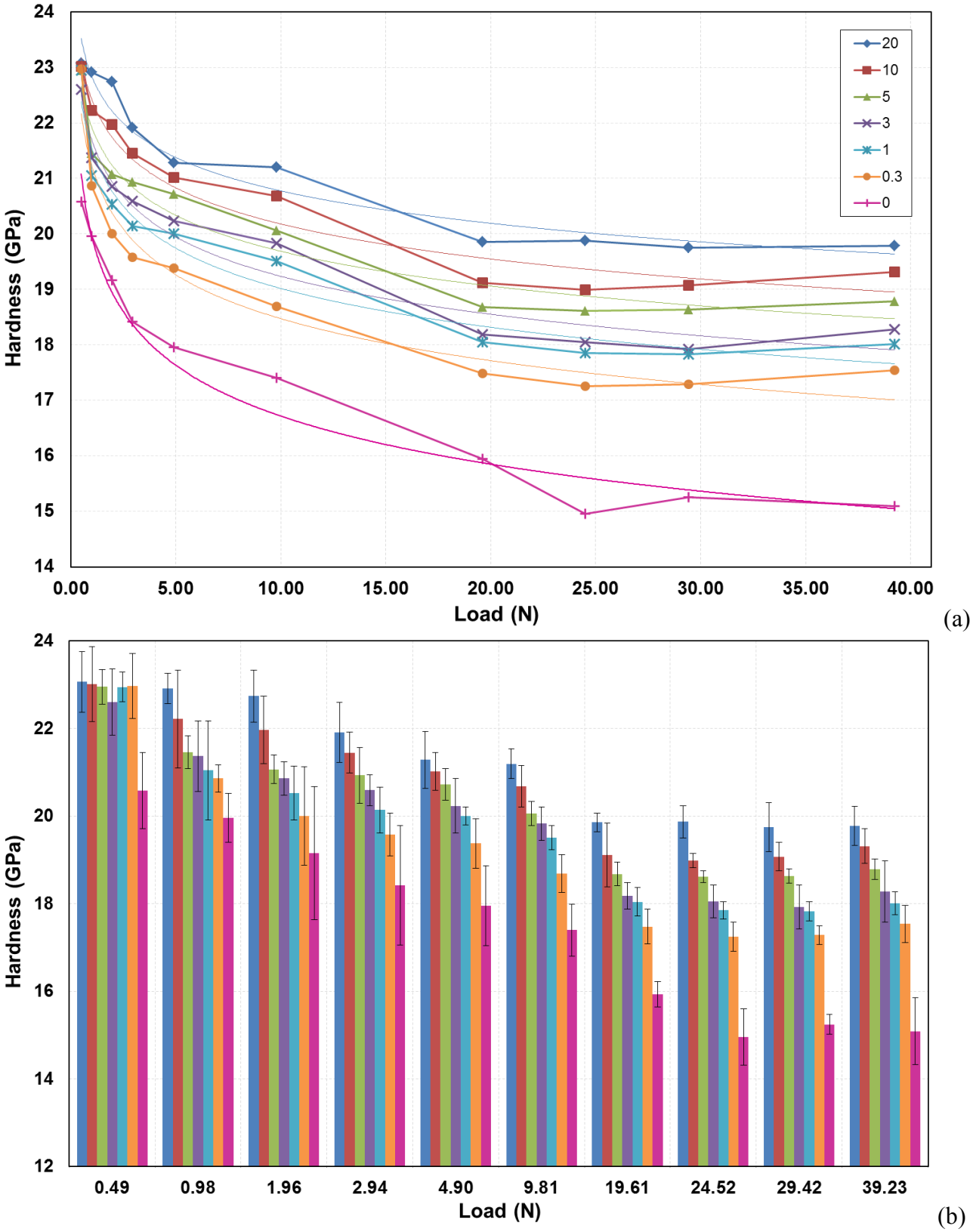

Figure 1: Hardness-load data for Al_2O_3 and Al_2O_3/SiC nanocomposites with different vol% SiC dispersants; (a) a line graph with power trendlines highlighting the ISE (b) a bar chart with error bars of one standard deviation.

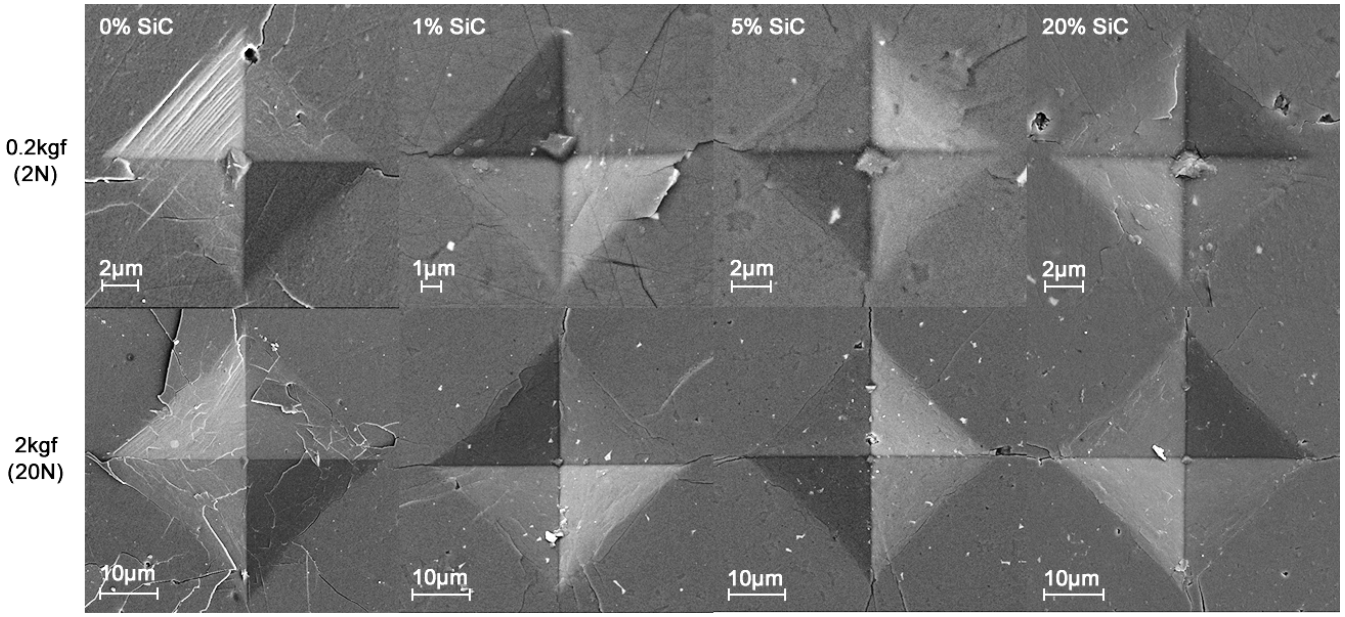

Figure 2: Representative SEM images of indents on samples containing 0, 1, 5 and 20vol%SiC at 0.2kgf (2N) and 2kgf (20N).

Another feature of the *H-P* graph worth noting is the maximum recorded hardness (H_{max}) of the Al_2O_3/SiC nanocomposite. At 0.5N (P_{min}) the numerical values of the H_{max} converge regardless of the SiC vol%, but immediately separate under greater loads. The circumstances of this have been rationalised by Lawn, Marshall and coworkers, who explain in a collection of papers that indents evolve from deformation-dominated behaviour to fracture-dominated behaviour above a certain critical load[24, 25, 26, 27]. In conjunction with this theory, we further speculate that at loads as low as 0.5N, with a penetration depth of ~1-2μm, the range of the dislocation activity would be limited to one single alumina grain. This constrains dislocation gliding to short ranges which likely facilitates work hardening, especially if cracking is not available to release the strain energy. The introduction of SiC nano-dispersants imposes further resistance leading to a higher hardness for the nanocomposites. It is possible, that as the load increases, cracking is initiated through the interactions between slip and the grain boundary or among the slips themselves, dissipating the built-up strain energy and prohibiting work hardening. We suspect further nanoindentation studies will disclose more detail on the converging effect of the hardness values at low loads.

Table 1: The numerical values of notable features in the hardness-load graph.

SiC (vol%)	H_{max} (GPa)	P_{max} (N)	H_{min} (GPa)	P_{min} (N)	$H_{plateau}$ (GPa)
0	20.58GPa	0.5	14.96	25	15.31
0.3	22.97GPa	0.5	17.25	25	17.39
1	22.95GPa	0.5	17.83	30	17.94
3	22.61GPa	0.5	17.93	30	18.11
5	22.95GPa	0.5	18.61	25	18.68
10	23.02GPa	0.5	18.99	25	19.12
20	23.07GPa	0.5	19.75	30	19.81

(a) Meyer's Law

The classical power law adopted to describe the *H-P* curves can be further applied to approximately quantify the severity of the ISE based on the value of the exponent or Meyer Index, *n*. In the absence of an ISE $n = 2$. In this scenario, Meyer's Law is modified to form Kick's Law[28]:

$$P = Ad^2 \tag{6}$$

where *P, d* and *A* are of equivalent significance as in Eq. 2. If $n < 2$ then the measured hardness decreases with an increasing load, indicating the presence of an ISE. In the rare case when $n > 2$ a reverse ISE behaviour is said to exist[17, 29].

In order to determine the *A*- and *n*-values through regression analysis, the Meyer's Law, defined in Eq. 2, is expressed in a logarithmic relationship:

$$\log P = \log A + n \times \log d \tag{7}$$

The resultant log*P* vs. log*d* graph is presented in Fig. 3 with the corresponding *A*- (intercept) and *n*-values (gradient) displayed in Table 2. By reviewing Fig. 3, a relatively high degree of linearity can be seen in each of the nanocomposites. However, the monolithic Al_2O_3 notably deviates at the higher applied loads of 20, 25, 30 and 40N. This may be attributable to measurement errors caused by the brittleness of Al_2O_3 which inhibited the precise dimensional assessment of the indents. Fig 1(b) supports this by highlighting the comparatively large error bars for pure Al_2O_3 at the aforementioned loads. Additionally, Fig. 2 visually illustrates the brittle nature of the unreinforced Al_2O_3, even at 2N. Nevertheless, overall, the results are consistent with previous studies[19].

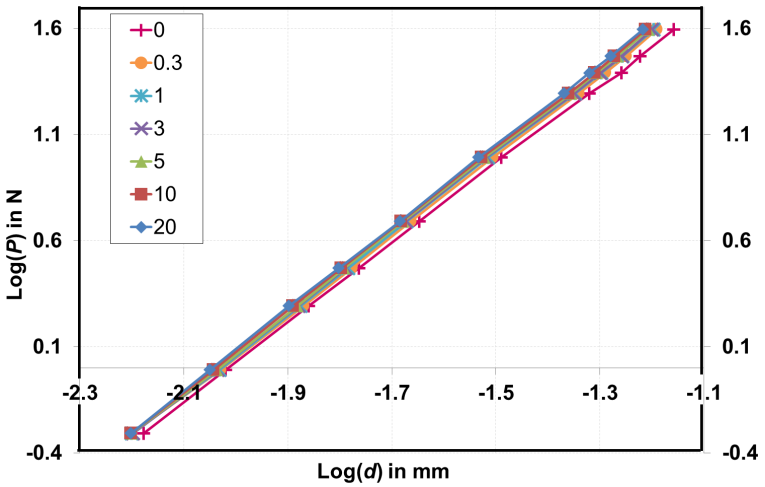

Figure 3: The log(load)-log(diameter) data for Al_2O_3 and Al_2O_3/SiC nanocomposites with different vol% SiC dispersants. Note the "kink" in the pure alumina curve across the higher load points.

From Table 2, a steady increase in the calculated *n*-values across all samples clearly demonstrates a substantial reduction in the ISE, particularly between the monolithic Al_2O_3 and the 0.3vol%SiC sample. More gradual changes are seen across the nanocomposites, with increasing SiC content correlating with a less pronounced ISE. The higher *n*-values also imply that the nanocomposites experience more ductile deformation during indentation with variations in the vol% of SiC nano-dispersants controlling the degree with which such deformation dominates. No direct relationship between the SiC vol% and the *n*-value is apparent, nor is there a synonymous relationship between *A* and *n* as described by Sargent and Page[4, 6].

Referring back to the $H_{plateau}$ in Table 1, Meyer's Law can be employed to affirm the observed levelling of the measured hardness. In accordance with Eq. 6, if the *n*-value across the narrower load range = 2 it implies that the ISE has disappeared. From the results for the $n_{plateau}$, presented in Table 2, it is apparent that the ISE has deteriorated to a negligible level in the SiC reinforced Al_2O_3 nanocomposites. However, the same cannot be said for the $n_{plateau}$ in the unreinforced Al_2O_3 which has

a value relatively similar to its original Meyer index and still significantly lower than the n-value of 0.3vol%SiC. Thus, it appears the ISE is still prevalent within the monolithic Al_2O_3 across the $H_{plateau}$ and that a levelling of the data collected is yet to occur.

Table 2: A summary of the n and A parameters determined using the Meyer's Law and the n-values calculated across a narrower load range of 20-40N ($H_{plateau}$).

	0vol%SiC	0.3vol%SiC	1vol%SiC	3vol%SiC	5vol%SiC	10vol%SiC	20vol%SiC
n	1.857	1.886	1.897	1.900	1.911	1.912	1.921
A	42.24	45.92	47.28	47.73	48.94	49.57	50.83
R^2	0.9998	0.9998	0.9999	0.9999	0.9999	0.9999	0.9999
$n_{plateau}$	1.869	2.013	2.000	2.010	2.017	2.035	1.985

(b) PSR Model

It is generally agreed that whilst Meyer's Law provides a reliable indication of the existence of an ISE, it is insufficient in interpreting its origin and is incapable of determining the "true hardness" when n does not equal 2. Consequently, the PSR model was composed[10, 11, 12], combining Kick's Law (Eq. 6), known to be the load-independent hardness (a_2d^2), and a modified version of Hays and Kendall's W constant, representing a materials resistance to the initiation of plastic flow, but that increases with indentation size and is directly proportional (a_1d).

By rearranging the PSR equation (Eq. 3) into the following

$$P/d = a_1 + a_2d \tag{8}$$

regression analysis can be employed to acquire the a_1- and a_2-values. Such data is presented in both the P/d-d graph (Fig. 4) and in numerical format in Table 3. Table 3 also displays the "true hardness" values (H_{PSR}) calculated by combing Eqs. 1 and 3 to formulate Eq. 9:

$$P = a_1d + (H/\alpha)d^2 \tag{9}$$

where α is the indenter specific constant for a Vickers indenter and equal to 1.8544.

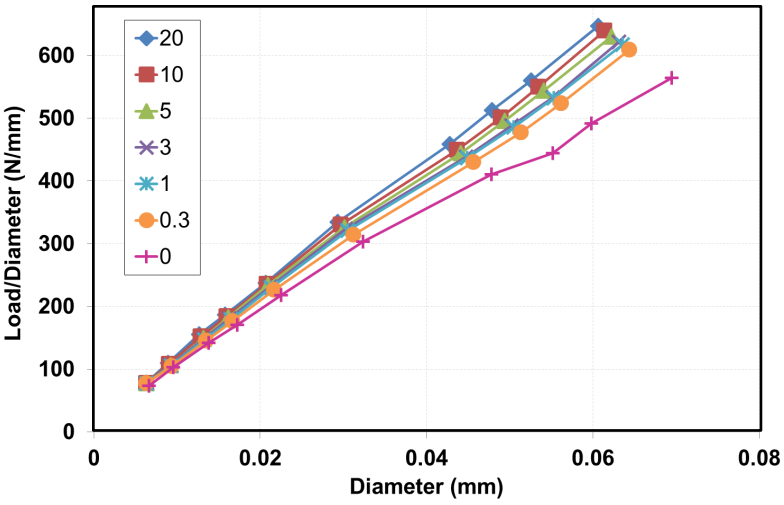

Fig. 4: The load/diameter-diameter data for Al_2O_3 and Al_2O_3/SiC nanocomposites with different vol% SiC dispersants.

The majority of the a_1-values obtained are in good agreement with the n-values derived using Meyer's Law. In both models, the largest sequential change is between the pure Al_2O_3 and 0.3vol%SiC nanocomposite. Similarly, incremental reductions in the ISE can be identified across all samples. However, magnified displays of nonlinearity result in a relatively lower correlation coefficient and irregularities in the a_1-values are seen at 3 and 10vol%SiC. At these points a_1 actually increases with further additions of SiC, rather than decreasing. The reason why this occurs is unknown.

Conversely, the a_2 term exhibits a favourable trend with regular increases in value related to higher vol% of SiC nano-dispersants.

Comprehension of the "true hardness" (H_{PSR}) determined from a_2 is exceedingly difficult as the numbers are lower than the H_{min} values displayed in Table 1. Several authors have produced complementary data[19, 20, 30, 31] with some concluding that it is only logical to reject "true hardness" values that are below experimental measurments[44].

Table 3: A summary of the a_1 and a_2 terms according to the PSR model in conjunction with the "true hardness" values.

SiC (vol%)	a_1	a_2	H_{PSR} (Gpa)	R^2
0	36.34	7648.53	14.19	0.9964
0.3	25.26	8957.12	16.61	0.9990
1	24.90	9255.86	17.16	0.9988
3	25.45	9344.53	17.33	0.9984
5	22.55	9696.22	17.98	0.9990
10	22.89	9931.37	18.42	0.9987
20	21.51	10299.41	19.10	0.9993

(c) MPSR model

In a series of papers, Gong reported various problems with the PSR model beyond those documented in this paper. These included the nonlinearity of the *P/d-d* curves and the "true hardness" across wider and narrower load ranges[13], and the inability to determine agreeable reverse ISE results[17]. As such, Gong deemed the PSR model unsatisfactory for explaining the ISE and made appropriate adjustments to form the MPSR model, defined in Eq. 4.

The application of this equation to the *H-P* data in Fig. 1 produces the *P-d* curves illustrated in Fig. 5. Values for a_0, a_1 and a_2 are evaluated through second order polynomial regression analysis and presented in Table 4.

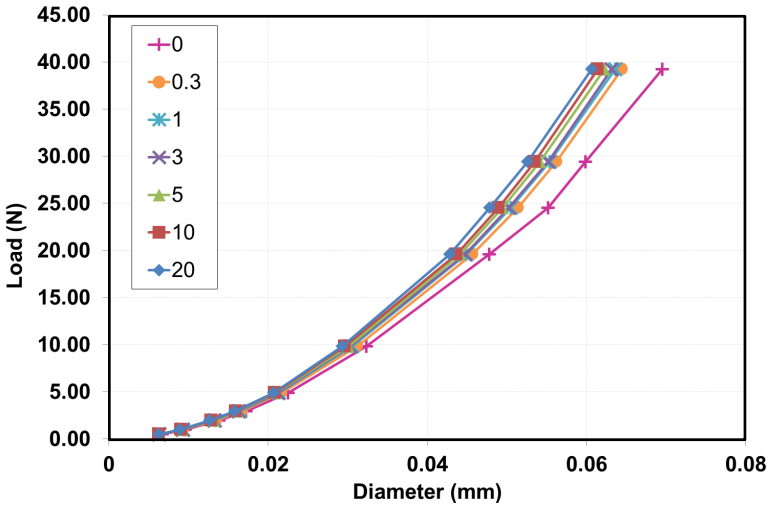

Fig. 5: The load-diameter data for Al_2O_3 and Al_2O_3/SiC nanocomposites with different vol% SiC dispersants.

The "true hardness" values for each of the samples have been estimated by substituting Eq. 1 into Eq. 4 generating Eq. 10 shown below:

$$P = a_0 + a_1 d + (H/\alpha)d^2 \quad (10)$$

In both of the MPSR equations (Eq. 4, Eq. 10), the addition of the a_0 term is said to account for the residual surface stresses caused by abrasive grinding/polishing and are strictly compressive. Hence, as Gong experienced, values of a_0 should be negative. In Table 4, a_0 for pure Al_2O_3 conforms to this assumption and even yields a numerical value consistent with Gong's initial study (a_0 = -0.3N)[13].

However, successive results for the nanocomposite shift from negative to positive to negative, or compression to tension to compression. This is inconsistent with our own surface residual stress measurements performed using luminescence spectroscopy[37]. Although, the data from the investigation

found significant fluctuations between compression and tension, it showed that Al_2O_3, with the same 1μm finish, has a net tensile residual stress whilst the Al_2O_3/SiC nanocomposite has a net compressive residual stress. This is contrary to the a_0-values obtained using the MPSR model.

It should be noted that Gong has since revised his original interpretation of the physical meaning of a_0 and currently associates it with experimental errors caused by the optical resolution tolerances of the objective lens used and/or the load accuracy of the indenter equipment. Regardless, the addition of the a_0 term achieves its intended purpose, to improve the correlation coefficient over varying load ranges. Evidently, there is scope for a further investigation into whether a physical meaning exists for a_0.

For a_1, a distinct differential between the unreinforced Al_2O_3 and the nanocomposite is apparent. However, as with a_0, the actual numerical values follow no discernable pattern.

As expected, the behaviour of a_2 is in accordance with the exponent, n, in Meyer's Law and the a_2 term in the PSR model. Once again, a substantial increase between the monolithic Al_2O_3 and the 0.3vol%SiC nanocomposite occurs with small, accumulative increases across the nanocomposites. Similarly, as observed in the PSR model, the calculated "true hardness" (H_{MPSR}) values determined from the a_2 data are less than experimental results.

Table 4: A summary of the a_0, a_1 and a_2 terms in accordance with the MPSR model together with the "true hardness" values and corresponding correlation coefficients.

SiC (vol%)	a_0	a_1	a_2	H_{MPSR} (Gpa)	R^2
0	-0.3291	72.72	7091.85	13.15	0.9995
0.3	0.1453	13.62	9115.74	16.90	0.9997
1	0.0202	26.28	9209.61	17.08	0.9997
3	0.0714	22.29	9364.11	17.36	0.9996
5	0.0725	18.45	9736.41	18.06	0.9998
10	0.1384	12.23	10074.92	18.68	0.9997
20	-0.0522	29.76	10143.35	18.80	0.9999

(e) Physical Interpretation of the Data

Having calculated the values for a_1 and a_2 using the PSR and MPSR models, it would seem appropriate to attribute some sort of physical significance to the terms.

For a_2, two key observations were made:

1. The initial introduction of SiC nanoparticles to the alumina matrix generated a large discrepancy between the a_2 values of the monolithic Al_2O_3 and the 0.3vol%SiC nanocomposite.

2. The subsequent additions of SiC nano-dispersants produced smaller incremental increases in the nanocomposite. We believe that two interrelated mechanisms are capable of controlling this trend.

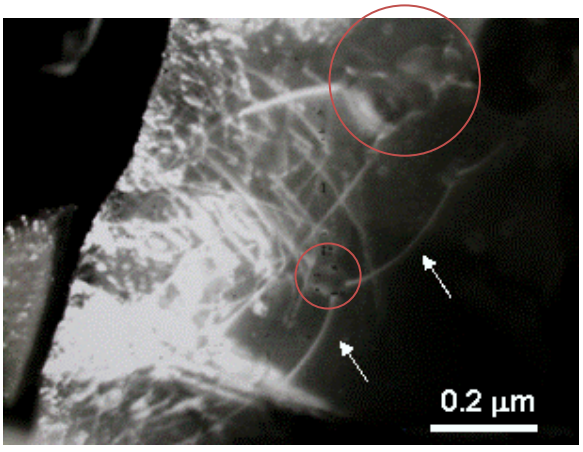

Fig. 6: Cross-section view of a grain underneath the polished surface of SiC nanocomposite. As arrowed, dislocations resort to bowing as silicon carbide nanoparticles impede there motion.

The first mechanism involves the dislocation density. In unreinforced Al_2O_3, the primary mode of deformation under external loading is basal twinning[32, 33]. Here, twins initiate at points of high stress, typically on the contact surface or grain

boundary, and grow through the grain until they hit the adjacent grain boundary. In the nanocomposite, nanoparticles prevent twins gliding whilst simultaneously acting as nucleation sites for dislocations[34, 35]. This is evidenced in TEM images given in earlier publications[34, 36] which show extensive basal twinning in pure Al_2O_3, whereas, the subsurface of the nanocomposite is dominated by dislocations without basal twins.

However, the mere presence of high dislocation densities at the surface is not enough to substantiate the previously described behaviour of the a_2 term. Thus, a second mechanism is necessary.

We propose that the nano-dispersion's capacity to resist the motion of dislocations is the underlying cause of variations in the measured hardness values displayed in Fig. 1. TEM examinations have demonstrated how SiC nanoparticles impede dislocations, causing them to bow, as indicated by the arrows in Fig. 6. The critical shear stress needed for this to occur is dictated by the lattice spacing of the nanoparticles within the Al_2O_3 matrix and controlled by the SiC particle size (inversely-proportional) and vol% (proportional). The maximum critical shear stress needed to bypass silicon carbide nanoparticles is given by[36]:

$$\Delta\tau = \frac{71.4 f^{1/3}}{(1.6 - 2f^{1/3})r} \tag{11}$$

where f represents the volume fraction and r is the radius of the particles. Following Tabor's approximation:

$$H \approx 3\sigma_y = 6\tau = H_0 + 6\Delta\tau \tag{12}$$

where H_0 is the true hardness of alumina and σ_y is the yield stress. The predicted H values of Eqs. 10 and 11 are plotted in Fig. 7 for dispersants sized between 25-200nm. The "true hardness" results generated by the MPSR model have been applied to determine their correlation.

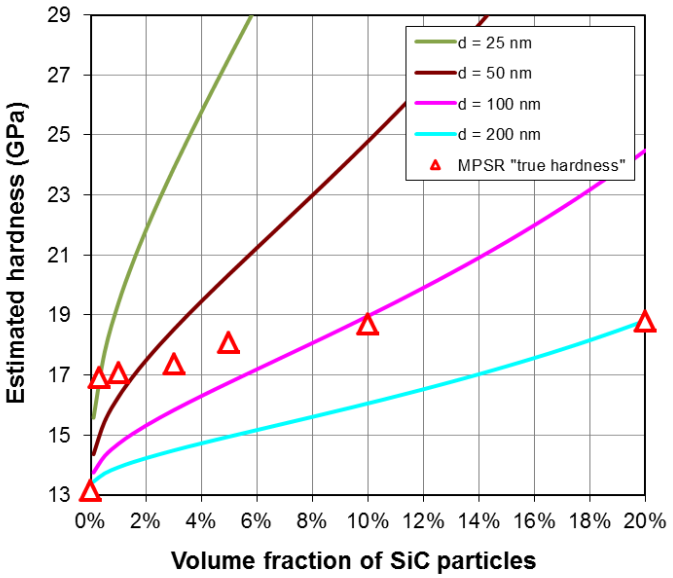

Fig. 7: The estimated hardness versus the particle size and volume percentage.

If we postulate that the SiC nano-particles are equally-sized and homogenously distributed throughout the matrix, than we would expect the "true hardness" data to fit the predictions. However, we must address the realities of ceramic powder processing. It is well known that lower vol% SiC dispersions are far more suitable for producing a uniform distribution throughout matrix and have a higher probability of maintaining a particle size close to that of the original crystallites. Whereas, in higher vol% dispersions, nanoparticles have a tendency to agglomerate into substantially larger, irregular clusters. This is illustrated in Fig. 6, which highlights nanoparticles of both 50-100nm and 200-300nm (circled) within the same microstructure. Consequently, the "true hardness" values derived from the MPSR model do not satisfy the predictions. Nevertheless, they act as a base from which the SiC dispersants distribution and population throughout the nanocomposite can be characterised.

For the *a1* term, little can be concluded based on the numerical values obtained from the PSR and MPSR models, particularly across the Al_2O_3/SiC. However, the randomness of the results combined with the notable difference between pure Al_2O_3 and the nanocomposite tends to suggest that fracturing is the direct cause of the ISE. The contrasting fracture mode of the Al_2O_3 in comparison with

the Al_2O_3/SiC could justify the large gap in the a_1 values and the unpredictable nature of crack initiation and crack propagation could explain the inconsistencies in the data. Future work will concentrate on validating this theory.

CONCLUSION

Hardness-load plots for ground and polished monolithic Al_2O_3 and Al_2O_3/SiC nanocomposites show that with further additions of SiC nano-reinforcements increases in the measured hardness and reductions in the severity of the ISE are to be expected. Meyer's Law, the PSR model and the MPSR model have all been proven insufficient in determining an acceptable "true hardness". Increases in dislocation density and the nano-dispersants capacity to resist the motion of dislocations are two mechanisms that have been proposed to explain apparent hardening of Al_2O_3/SiC nanocomposite.

REFERENCES

[1] Smith, R. & Sandland, G. An accurate method of determining the hardness of metals, with particular reference to those of a high degree of hardness. *Proceedings of the Institution of Mechanical Engineers*. 1922, **102** (1), pp. 623-641.

[2] Amprino R. Investigations on some physical properties of bone tissue. *Acta Anatomica*. 1958, **34** (3), pp. 161-186.

[3] Quinn, J. & Quinn, G. Indentation brittleness of ceramics: a fresh approach. *Journal of Materials Science.* 1997, **32** (16), pp. 4331-4346.

[4] Sargent, P. & Page, T. Influence of microstructure and microhardness of ceramic materials. *Proceedings of the British Ceramic Society*. 1978, **26**, pp. 209-234.

[5] Czernuszka, J. & Page, T. Characterizing the surface contact behaviour of ceramics: Part 1 Hardness response of glass-bonded Al2O3 and titania. *Journal of Materials Science*. 1987, **22** (11), pp. 3907-3916.

[6] Li, H. & Bradt, R. The microhardness indentation load/size effect in rutile and cassiterite single crystals. *Journal of Materials Science*. 1993, **28** (4), pp. 917-926

[7] Gong, J., Wu, J. & Guan, Z. Analysis of the indentation size effect on the apparent hardness for ceramics. *Materials Letters*. 1999, **38** (3), pp. 197-201.

[8] Hays, C. & Kendall, E. An analysis of Knoop microhardness. *Metallurgy*. 1973, **6** (4), pp. 275–282.

[9] Tarkanian, M., Neumann, J. & Raymond, L. Determination of the temperature dependence of {1 0 0} and {1 1 2} slip in tungsten from Knoop hardness measurements. In: Westbrook, J. & Conrad, H. *The science of hardness testing and its research applications*. American Society for Metals, Ohio, USA, 1973, pp. 187–198.

[10] Bernhardt, E. Über die Mikrohärte der Feststoffe im Grenzbereich des Kick'schen. Ähnlichkeitssatzes. *Zeitschrift für Metallkunde*. 1941, **33**, pp. 135.

[11] Frohlich, F., Grau, P. & Grellmann, W. Performance and analysis of recording microhardness tests. *Physica Status Solidi A*. 1977, **42** (1), pp. 79-89.

[12] Li, H. & Bradt, R. The indentation load/size effect and the measurement of the hardness of vitreous silica. *Journal of Non-Crystalline Solids*. 1992, **146**, pp. 197-212.

[13] Gong, J., Wu, J. & Guan, Z. Examination of the indentation size effect in low-load vickers hardness testing of ceramics. *Journal of the European Ceramic Society*. 1999, **19** (15) pp. 2625–2631.

[14] Carpinteri, A. & Puzzi, S. A fractal approach to indentation size effect. *Engineering Fracture Mechanics*. 2006, **73** (15), pp. 2110–2122.

[15] Meyer, E. Untersuchungen über Harteprufung und Harte. *Zeitschrift fur Physik*. 1908, **9**, pp. 66–74.

[16] Hirao, K. & Tomozawa, M. Microhardness of SiOz glass in various environments. *Journal of the American Ceramic Society*. 1987, **70** (7), pp. 497-502.

[17] Gong, J., Miao, H., Zhao, Z. & Guan, Z. Load-dependence of the measured hardness of Ti(C,N)-based cermets. *Materials Science and Engineering: A*. 2001, **303** (1–2), pp. 179–186.
[18] Kim, H. & Kim, T. Measurement of hardness on traditional ceramics. *Journal of the European Ceramic Society*. 2002, **22** (9-10), pp. 1437–1445.
[19] Csehová, E., Andrejovská, J., Limpichaipanit, A., Dusza, J. & Todd, R. Indentation load-size effect in Al_2O_3-SiC nanocomposites. *Journal of Electrical Engineering*. 2010, **61** (5), pp 305-307.
[20] Machaka, R., Derry, T., Sigalas, I. & Herrmann, M. Analysis of the indentation size effect in the microhardness measurements in B6O. *Advances in Materials Science and Engineering*. 2011, **2011**, pp. 1-6.
[21] Li, H., Ghoshs, A., Han, Y. & Bradt, R. The frictional component of the indentation size effect in low load microhardness testing. Journal of Materials Research. 1993, **8** (5), pp. 1028-1032.
[22] Weppelmann, E., Wittling, M., Swain, M. & Munz, D. Indentation cracking of brittle thin films on brittle substrates. In: Bradt, R., Hasselman, D., Munz, D., Sakai, M. & Shevchenko, Y. *Fracture mechanics of ceramics*. Plenum Press, New York, USA, 1996, pp. 475-486.
[23] Wu, H., Lawrence, C., Roberts, S. & Derby, B. The strength of Al_2O_3/SiC nanocomposites after grinding and annealing. *Acta Materialia*. 1998, **46** (11), pp. 3839-3848.
[24] Lawn, B. & Marshall, D. Hardness, toughness and brittleness: An indentation analysis. *Journal of the American Ceramic Society*. 1979, **62** (7-8), pp. 347-350.
[25] Marshall, D. & Lawn, B. Indentation of Brittle Materials, In: Blau, P. & Lawn, B. *Microindentation Techniques for Materials Science and Engineering*, American Society for Test Materials, Philadelphia, Pennsylvania, USA, 1986, pp. 26-40.
[26] Lawn, B., Jensen, T. & Arora, A. Brittleness as an indentation size effect. *Journal of Materials Science*. 1976, **11** (3), pp. 573-575.
[27] Lawn, B. & Evans, A. A model for crack initiation in elastic/plastic indentation fields. *Journal of Materials Science.* 1977, **12** (11), pp. 2195-2199.
[28] Kick, F. *Das gesetz der proportionalen widerstände und seine anwendung.* Felix, Leipzig, Germany, 1885.
[29] Sangwal, K. On the reverse indentation size effect and microhardness of solids. *Materials Chemistry and Physics*. 2000, **63** (2), pp. 145-152.
[30] Ćurković, L., Rede, V. & Grilec, K. Indentation size effect on the hardness of silicon carbide ceramics. *Kemija u Industriji*. 2010, **59** (10), pp. 483-488.
[31] Şahin, O., Uzun, O., Kölemen, U. & Uçar, N. Analysis of ISE in dynamic hardness measurements of β-Sn single crystals using a depth-sensing indentation technique. *Materials Characterization*. 2008, **59** (6), pp. 729-736.
[32] Wu, H., Roberts, S. G. & Derby, B. Residual stress and subsurface damage in machined alumina and alumina/silicon carbide nanocomposite ceramics. *Acta Materialia*. 2001, **49** (3), pp. 507-517.
[33] Inkson, B. Dislocations and twinning activated by the abrasion of Al_2O_3. *Acta Materialia*. 2000, **48** (8), pp. 1883-1895.
[34] Wu, H., Inkson, B. & Roberts, S. Subsurface deformation of machined Al_2O_3 and Al_2O_3/5vol%SiC nanocomposite. *Journal of Microscopy*. 2001, **201** (2), pp. 212-220.
[35] Levin, I., Kaplan, W., Brandon, D. & Wieder, T. Residual-stresses in alumina-sic nanocomposites. *Acta Metallurgica Et Materialia*. 1994, **42** (4), pp. 1147-1154.
[36] Wu, H., Roberts, S. & Derby, B. Ductile deformation in alumina/silicon carbide nanocomposites. In: Mathur, S., Singh, M., Singh, D. & Salem, J. *Nanostructured Materials and Nanotechnology III*, John Wiley & Sons, Inc, Hoboken, New Jersey, USA, 2010, pp. 155-163.
[37] Wu, H., Roberts, S. & Winn, A. Residual stress determination and subsurface microstructure in ground and polished alumina/silicon carbide nanocomposites and monolithic alumina ceramics. *Nanophase and Nanocomposite Materials III - Materials Research Society Symposium Proceedings*. 2000, 581, pp. 303-308.